Fusion Engineering and Design 87 (2012) 325–331

Contents lists available at SciVerse ScienceDirect

Fusion Engineering and Design

journal homepage: www.elsevier.com/locate/fusengdes

Simulation of EAST off-axis neutral beam heating and current drive

Zhongjing Chen[a], Tieshuan Fan[a,*], Cheng Zhang[a,b], Chundong Hu[b], Xiaogang Wang[a,*]

[a] School of Physics and State Key Laboratory of Nuclear Physics and Technology, Peking University, Beijing 100871, China
[b] Institute of Plasma Physics, Chinese Academy of Sciences, Hefei 230031, China

ARTICLE INFO

Article history:
Received 8 December 2011
Received in revised form 21 January 2012
Accepted 30 January 2012
Available online 25 February 2012

Keywords:
Off-axis
NBI
EAST
NUBEAM

ABSTRACT

The capability of off-axis neutral beam heating and current drive has been investigated with NUBEAM for Experimental Advanced Superconducting Tokamak (EAST). Three different approaches to realize off-axis Neutral Beam Injection (NBI) have been studied. Simulation results for on- and off-axis NBI are reported. The effects of the alignment of NBI relative to the magnetic field pitch on off-axis neutral beam heating and current drive are observed and discussed qualitatively. By comparing the numerical results, a most favorable off-axis NBI configuration is recommended. The capability to control sawtooth is also investigated by comparing locations of the $q = 1$ rational surface and the peak of the fast ion density profile.

1. Introduction

Neutral Beam Injection (NBI) has been widely used in tokamaks, such as DIII-D, JET, ASDEX-U, MAST, JT-60U and ITER in the future, as one of the main auxiliary heating and current drive (CD) methods. Since neutral beam CD (NBCD) is a noninductive CD, it plays a significant role in steady-state operation for which full-noninductive CD is required. In order to reach steady-state operation, the current profile must be controlled and optimized by a flexible, localized and efficient source of noninductive current. NBCD is one of the options for accomplishing this task.

The capability of utilizing the off-axis NBCD for advanced operation scenario development in ITER has been investigated by joint experiments [1] in four tokamaks (ASDEX-U [2–4], MAST [3,4], DIII-D [5,6] and JT-60U [7]). In ASDEX-U and DIII-D, it was found that better agreement could be reached when an anomalous fast ion diffusion coefficient of $D_b \sim 0.3$–$0.5\ m^2\ s^{-1}$ was introduced at high heating power (5 MW and 7.2 MW). Reasonable agreement between the measured and calculated (with $D_b \sim 0$–$0.5\ m^2\ s^{-1}$) NBCD related physical quantities in all of the tokamak plasmas without magnetohydrodynamic (MHD) activities, except ELMs, have been published [1–7]. In JET [8], ASDEX-U and MAST [9], the experimental results showed that it is possible to control sawtooth by off-axis NBI with an off-axis peaked fast ion distribution.

A main research goal of Experimental Advanced Superconducting Tokamak (EAST) is to demonstrate long duration discharge (1000 s) sustained by noninductive current drive. Lower hybrid current drive (LHCD) and ion cyclotron resonance heating (ICRH) are the two main auxiliary heating and current drive methods employed in EAST at present [10]. The NBI systems are under construction. The numerical results of plasma behavior under NBI with typical designed parameters (on-axis NBI) and variable profiles of density and temperature have been reported in [11]. The influence of the injection angle on the neutral beam (NB) heating and CD has also been investigated by simulation in [12]. However, off-axis NB heating and CD have not been considered until now. In this work, detailed simulations of off-axis NB heating and CD with $D_b = 0\ m^2\ s^{-1}$ are reported. Three different approaches to achieve off-axis NBI are considered. The effects of the alignment of NBI [6] relative to the magnetic field pitch are investigated by utilizing different combinations of the toroidal magnetic field B_t and the NB injection direction.

In Section 2, we give a brief introduction to EAST, its NBI system and simulation models. The three different methods for realizing off-axis NBI are also discussed. Detailed numerical results are presented and analyzed in Section 3, including discussions about the effects of the alignment of NBI relative to the magnetic field pitch and the capability of controlling MHD instabilities. Section 4 summarizes the main points of the study.

2. The EAST NBI system and simulation model

2.1. The EAST NBI system

EAST is a full super-conducting tokamak and the first discharge was achieved in 2006. LHCD and ICRH are currently used as

* Corresponding authors.
E-mail addresses: tsfan@pku.edu.cn (T. Fan), xgwang@pku.edu.cn (X. Wang).

0920-3796/$ – see front matter © 2012 Elsevier B.V. All rights reserved.
doi:10.1016/j.fusengdes.2012.01.046

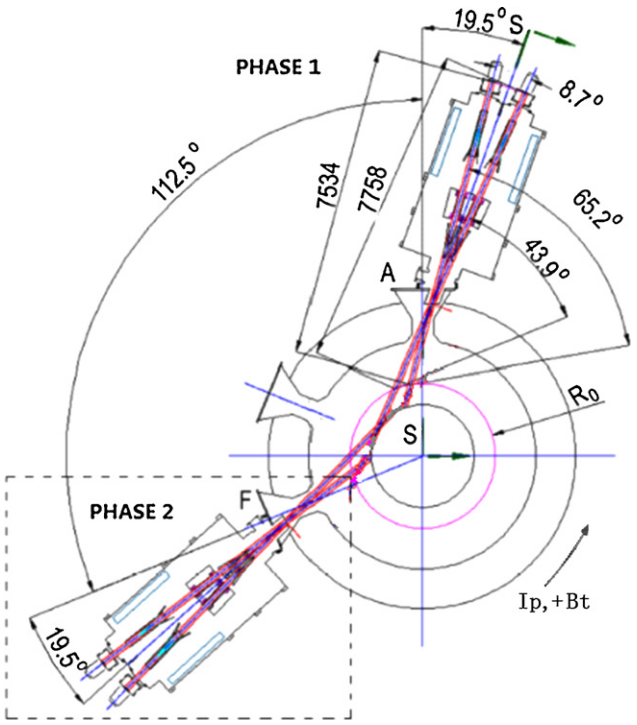

Fig. 1. The sketch of NBI system in EAST. Phase 2 will be constructed after Phase 1 is installed. The beam line with larger tangential radius is beamline 1, while that with smaller tangential radius is beamline 2. The direction of I_p and $+B_t$ is counter-clockwise.

auxiliary heating and CD methods. The typical operating parameters of EAST are as follows: the major radius $R_0 = 1.7$ m, the minor radius $a = 0.40$ m, elongation $\kappa = 1.6$–2.0, triangularity $\delta = 0.5$–0.7 and toroidal magnetic field $B_t = 3.5$ T [13]. The designed NBI system in EAST consists of two deuterium beamlines [14] with beam power $P_{\mathrm{nbi}} = 2$–4 MW for Phase 1 (see Fig. 1). It will be possible to double the beam power after Phase 2 is installed. The beam energy is 50–80 keV, and the injection energy fraction E:E/2:E/3 is 80%:14%:6%. The ion source shape and aperture shape are both rectangular. The half-width and half-height of the ion source are 6.0 cm and 24.0 cm, and the half-width and half-height of the aperture are 8.85 cm and 24.0 cm. The horizontal divergence is 0.6°, and the vertical divergence is 1.2°. The sketch of the injection angle and pitch angles is shown in Fig. 1.

2.2. Simulation models and code

There are commonly used two approaches to realize off-axis NB heating and CD in the joint experiments [1]: first, up/down shift of plasma employed in DIII-D and MAST; second, up/downward steered off-axis beams employed in ASDEX-U and JT-60U. KSTAR [15] offers a third approach, i.e., beam footprints vertically separated by rotating the ion sources. In this paper, we investigate all three methods in EAST. The poloidal plasma cross-section with the different configurations of the two ion sources is shown in Fig. 2. Type A (Fig. 2(a)) is the typical NBI system for on-axis heating and CD. The two beamlines are horizontally separated with the tangential radius $R = 134$ cm (beamline 1) and $R = 78$ cm (beamline 2), respectively. Type B (Fig. 2(b)), type C (Fig. 2(c)) and type D (Fig. 2(d)) are the three methods for achieving off-axis NBI heating and CD. The axes of the beam lines are drawn in Fig. 2(e). For type B, the beamlines are vertically separated with the tangential radius $R = 134$ cm by rotating the two ion sources which are remained up–down symmetric. The two beamlines are both off-axis, downward for the upper ion source and upward for the lower ion source. For type C, we up/down shift the ion sources, together with the beamlines, just like down/up shift of the plasmas in DIII-D and MAST. Up/downward steered off-axis beams are realized by type D by up/down shift of the ion sources while keeping the point of intersection of the two beamlines in the mid-plane. For beamline 1, the footprint is the same as the footprint of type B. Because the ion sources and the apertures are rectangular, there are distinctive differences in the numerical results as demonstrated in Section 3. We change the direction of toroidal magnetic field B_t to investigate the effects of the alignment of NBI relative to the magnetic field pitch on off-axis NB heating and CD. Co-/counter- (in the direction of/in the direction opposite to the plasma current) NBI are also considered.

NUBEAM [16,17], a subroutine for NB heating and CD calculation in ONETWO [18] transport code, is utilized in this work. ONETWO has been developed by General Atomics for experimental data analysis and the numerical simulation for tokamak geometries. It solves the flux surface averaged transport equations for energy, particles, toroidal rotation and current density with self-consistent source and sink simulation. An EFIT standard eqdsk type file of MHD equilibrium and plasma parameter profiles of EAST were used to start the simulation. The plasma current and toroidal magnetic field are 1 MA and 3.5 T, respectively. The plasma current and $+B_t$ are in the counter-clockwise direction. The magnetic pitch angle profile and safety factor q profile are shown in Fig. 3. The effective charge Z_{eff} is 2.0. The temperature and density profiles are assumed to have the following forms:

$$T(\rho) = [T(0) - T(1)](1 - \rho^2) + T(1),$$

$$n(\rho) = [n(0) - n(1)](1 - \rho^2)^{0.5} + n(1),$$

where ρ is a normalized flux surface coordinate, proportional to the square root of the enclosed toroidal magnetic flux. We assume $n(1) = 0.1n(0)$ and $T(1) = 0.1T(0)$. $T_e = T_i$ is assumed, and the center values of temperature and electron density are taken as 3 keV and 3.5×10^{19} m^{-3}, respectively.

3. Simulation results and discussions

In this section, on- and off-axis NB heating and CD are analyzed and compared, and the most favorable approach to realize off-axis NBI is identified for EAST. For each source, the beam power is 2 MW and the beam energy is 80 keV. By investigating the effects of the alignment of NBI relative to the magnetic field pitch on off-axis NB heating and CD, we find that the profiles of off-axis NBCD is sensitive to the alignment and there are favorable combinations of the toroidal magnetic field B_t and NB injection direction. The capability to control MHD instabilities, such as sawtooth, is also discussed.

3.1. The most favorable approach for achieving off-axis NB heating and CD in EAST

We present the simulation results of NB heating and CD for all the four types of NBI in the following paragraphs. For each type, we consider co-/counter- NBI, as well as positive/negative (in the direction of/in the direction opposite to the plasma current) B_t. For type A, C and D, only the beamline 1, which is a favorable beamline for NB heating and CD, as shown in [12] and the following discussions, is considered.

The simulation results of NB heating and CD for type A are shown in Fig. 4. Fig. 4(a) displays the power deposition. We can see that for all scenarios, the profiles of power deposition to ions and electrons are nearly centrally peaked. More NBI power is deposited to ions than to electrons, i.e., about 50% to ions and 25% to electrons. The

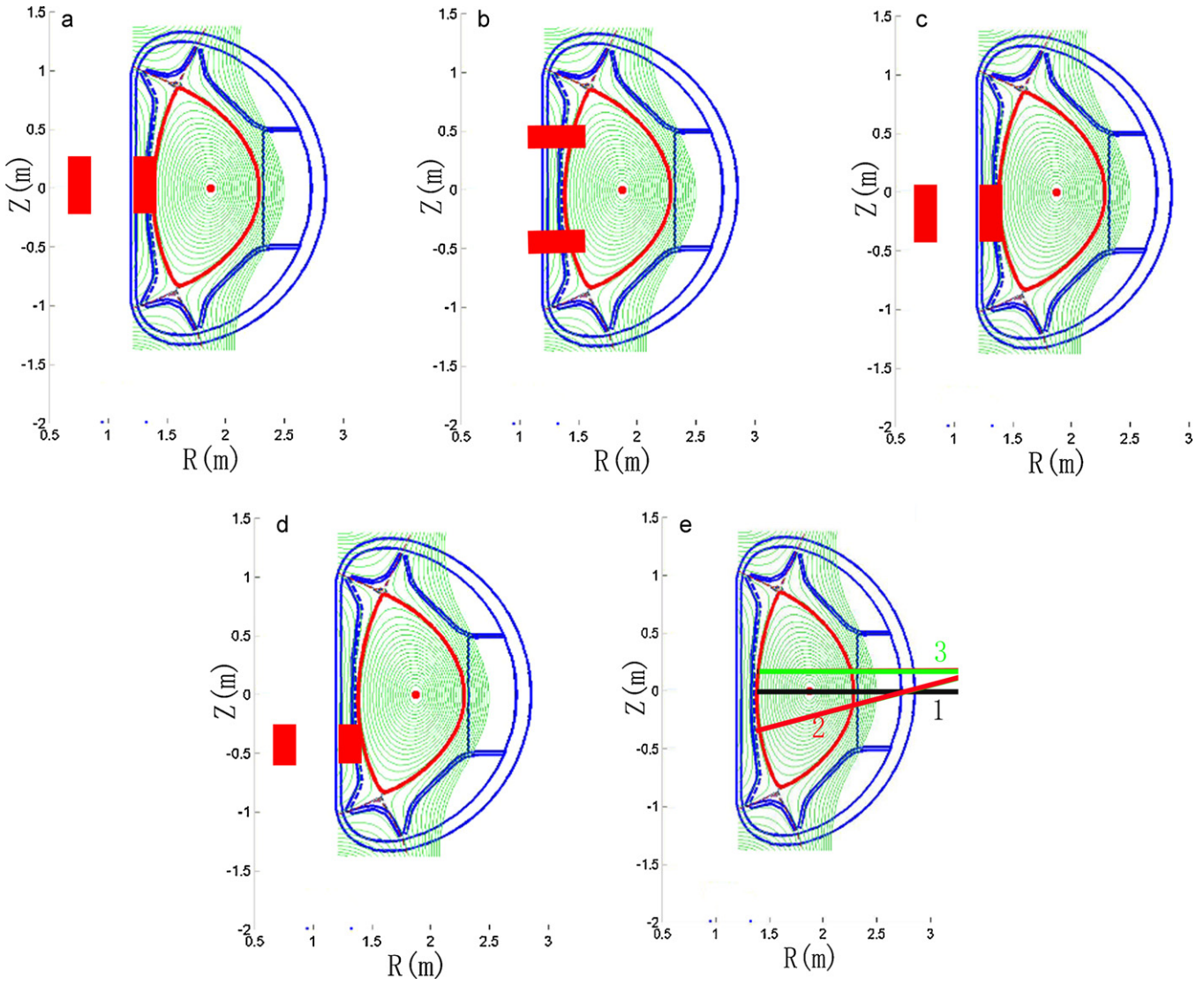

Fig. 2. The poloidal plasma cross-section with the two ion sources. Type A (a) is the original designed on-axis NBI, while type B (b), C (c) and D (d) are the three different approaches to realize off-axis NB heating and CD. The ion source located at $R = 134$ cm belongs to beamline 1 while the ion source located at $R = 78$ cm belongs to beamline 2. For type D, the poloidal cross-section heights of the ion sources decrease as they are steered. The axes of the beam lines are drawn in (e) with line 1 (black) for type A, line 2 (red) for type B and D, and line 3 (green) for type C. (For interpretation of the references to color in this figure legend, the reader is referred to the web version of the article.)

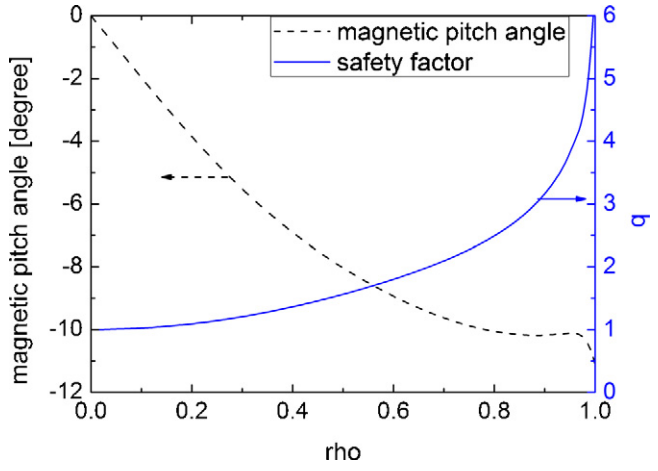

Fig. 3. The magnetic pitch angle profile (dashed and black) and the safety factor q profile (solid and blue). (For interpretation of the references to color in this figure legend, the reader is referred to the web version of the article.)

total power deposition for co-NBI is larger than that for counter-NBI. The main power loss mechanics for co-NBI are about 16% for shine-through, 5% for internal charge exchange and 3% for scrape-off region charge exchange. For counter-NBI, the scrape-off region charge exchange increases to 5% while the amounts of the other two mechanics are the same as those for co-NBI. Moreover, the bad orbits loss becomes one of the main power loss mechanisms, i.e., about 5%. The cooling and armor on the footprint portions of the EAST wall is required for co-NBI, while the energy dump of the divertor should also be considered for counter-NBI.

The profiles of NBCD are shown in Fig. 4(b). They are nearly centrally peaked and the driven plasma currents are about 0.045 MA/MW and −0.035 MA/MW for co- and counter-NBI respectively. Therefore, co-NBI is better for NB heating and CD. Due to the symmetry for on-axis NBI, changing the direction of toroidal magnetic field does not affect the power deposition and NBCD according to the following discussions.

Fig. 5 shows the simulation results for type B. The profiles of power deposition to electrons and ions are shown in Fig. 5(a) and (b), respectively. The profiles of power deposition peak off-axis at

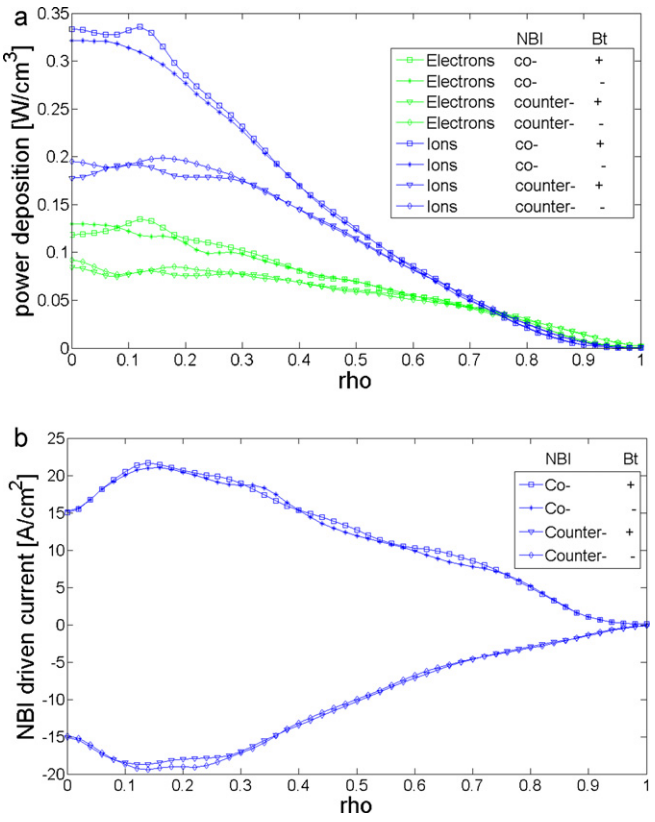

Fig. 4. The profiles of NBI power deposited (a) to electrons (green, solid) and ions (blue, dashed) and the profiles of NBCD, (b) for type A with co-/counter-NBI and positive/negative toroidal magnetic field B_t. (For interpretation of the references to color in this figure legend, the reader is referred to the web version of the article.)

$\rho = 0.2$–0.4. The ratios of the beam power deposited to ions and electrons are the same as in the cases of type A; that is, about 50% to ions and 25% to electrons. Unlike type A, however, the NB heating and CD are sensitive to the alignment of NBI relative to the magnetic field pitch. Therefore, there are favorable combinations of the toroidal magnetic field B_t and the NB injection direction. Considering the up–down symmetry of the equilibrium, there is always a downward off-axis NBI corresponded to each upward off-axis NBI as seen in Fig. 5. The profiles of NB heating and CD are almost the same for each pair. Considering co-NBI, the favorable combinations for NBCD are different from those for NB heating. The favorable combinations are $+B_t$/down (beamline is downward off-axis) and $-B_t$/up (beamline is upward off-axis) for NBCD and $-B_t$/down and $+B_t$/up for NB heating. From Fig. 5(c), we can see that the profiles of NBCD for favorable combinations peak off-axis at $\rho = 0.4$ and are reasonably localized, while the profiles for unfavorable combinations peak off-axis at $\rho = 0.35$ and are also reasonably localized. The magnitudes of NBCD with favorable combinations are higher than those with unfavorable combinations and the total values of NBCD are about 0.049 MA/MW and 0.042 MA/MW for favorable and unfavorable combinations, respectively.

The reasons for the existence of favorable combinations were illustrated qualitatively in [5,6]. Specially, the differences of fast ion trapping fraction and electron shielding (cancellation) current, which decreases with radius due to trapping of electrons are responsible for the existence of favorable combinations. In the case of favorable combinations for NBCD, the beamline has a smaller pitch angle and more deposited beam ions become passing particles. In contrary, for unfavorable combinations, more deposited beam ions become trapped particles because the beamline has a larger pitch angle. Since trapped particles are born on the outer legs of their banana orbits during co-NBI and the banana widthis

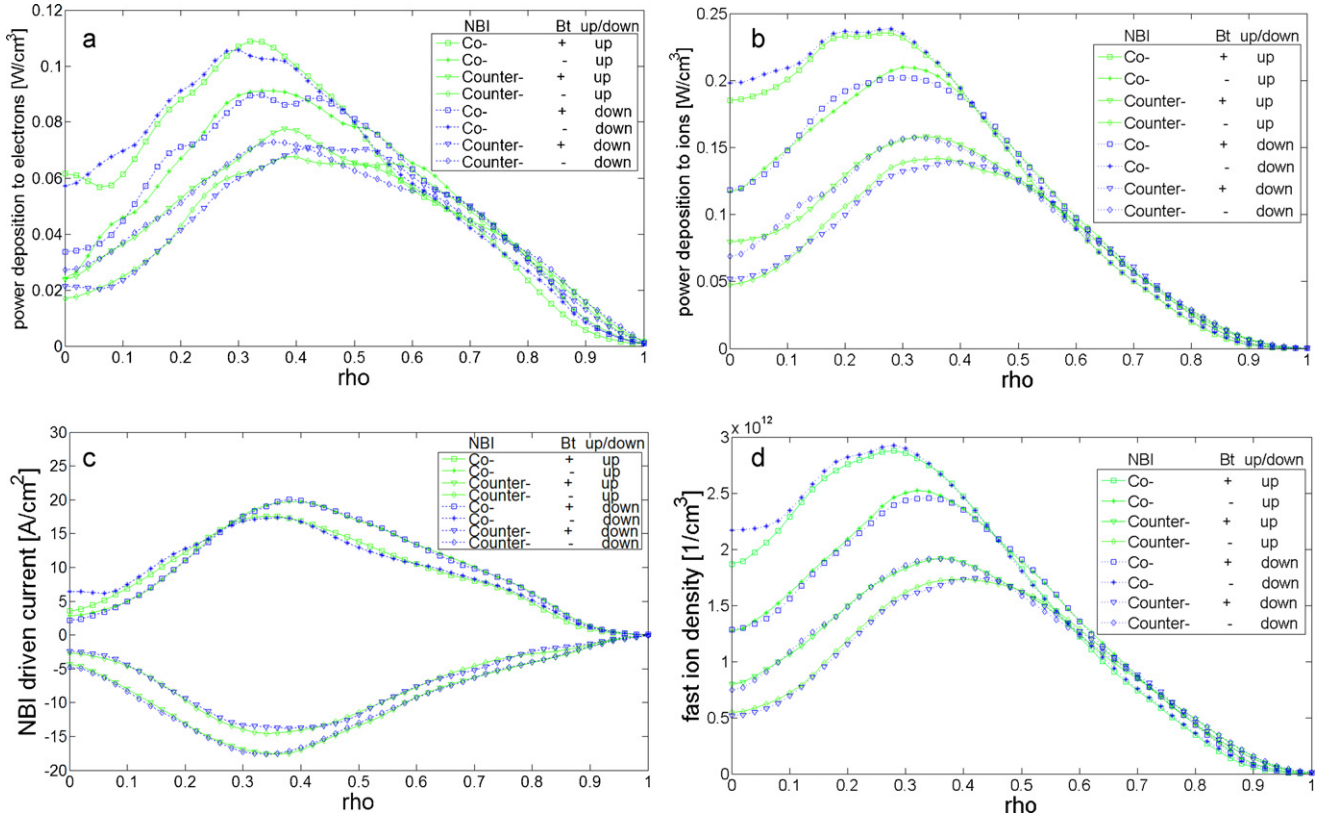

Fig. 5. The profiles of NBI power deposited to electrons (a) and ions, (b) and the profiles of NBCD, (c) and fast ion density, (d) for type B with co-/counter-NBI and positive/negative toroidal magnetic field B_t. Up (green, solid)/downward (blue, dashed) off-axis NBIs are separately considered. (For interpretation of the references to color in this figure legend, the reader is referred to the web version of the article.)

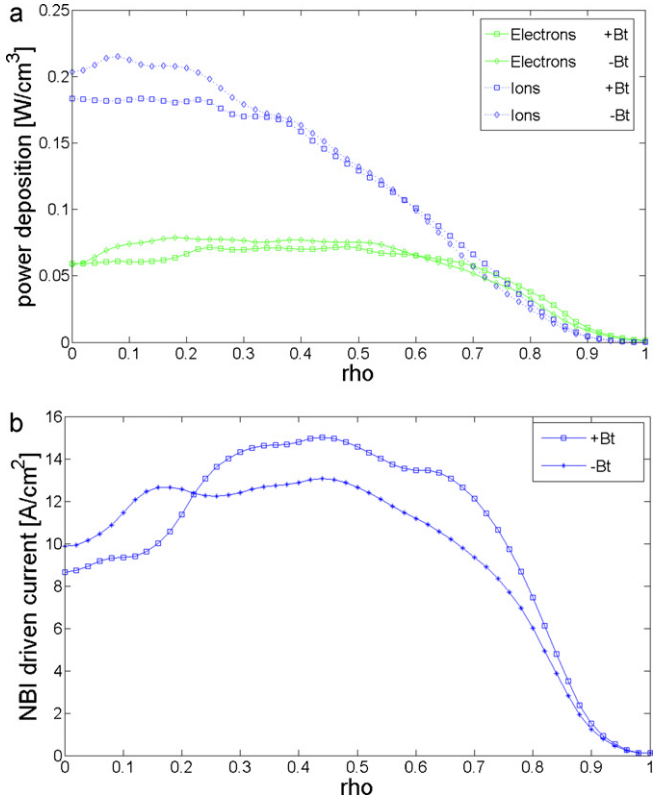

Fig. 6. The profiles of NBI power deposited (a) to electrons (green, solid) and ions (blue, dashed) and the profiles of NBCD, (b) for type C with co-NBI and positive/negative toroidal magnetic field B_t. (For interpretation of the references to color in this figure legend, the reader is referred to the web version of the article.)

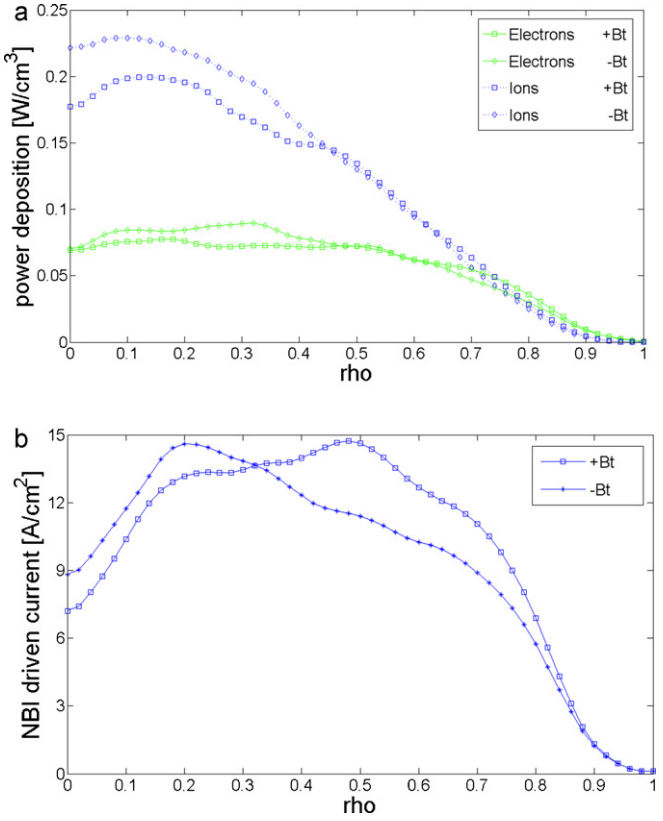

Fig. 7. The profiles of NBI power deposited (a) to electrons (green, solid) and ions (blue, dashed) and the profiles of NBCD, (b) for type D with co-NBI and positive/negative toroidal magnetic field B_t. (For interpretation of the references to color in this figure legend, the reader is referred to the web version of the article.)

large near the magnetic axis, thus the fast ion density for unfavorable combinations near the axis is larger than that for favorable combinations, as shown in Fig. 5(d). As passing fast ions circulate more frequently around the torus than the trapped ions, they can more effectively build up fast ion current. Moreover, in the case of passing electrons, they move along with the passing ions and introduce a shielding current that reduces the fast ion current. However, this reduction does not happen for trapped electrons. Therefore, the magnitudes of NBCD with favorable combinations are higher while the current density near the magnetic axis is higher for unfavorable combinations (as seen in Fig. 5(c)).

For counter-NBI, the favorable combinations for NB heating and CD are the same, i.e., $+B_t$/up and $-B_t$/down, which are the unfavorable combinations for NBCD of co-NBI. The counter beams produce more trapped particles than co beams [19]. Trapped particles are born on the inner leg of their banana orbit during counter-NBI, so the first-orbit losses increase [20]. Because of the large banana width near the magnetic axis, the profiles of fast ion density for unfavorable combinations whose beam pitch angles are large move outward and the magnitudes are lower as shown in Fig. 5(d). Moreover, for co-NBI, the fast ions are better confined and the total NB driven current is higher, about 0.049 MA/MW and 0.042 MA/MW for favorable and unfavorable combinations with co-NBI and 0.040 MA/MW and 0.032 MA/MW for favorable and unfavorable combinations with counter-NBI.

For type C and type D, the properties of the profiles of NB heating and CD are almost the same as for type B. Here, we present only the results of down-shift 20 cm and down-steered off-axis co-NBI in Figs. 6 and 7, respectively. The profiles of NBI power deposition are nearly the same and flattened near the magnetic axis for both types. However, the profiles of NBCD are different. For type C, the profiles of NBCD do not have obvious peaks. They are nearly flattened in the range of $\rho = 0.3$–0.5 and $\rho = 0.15$–0.55 for favorable and unfavorable combinations, respectively. The profiles of NBCD for type D peak off-axis at $\rho = 0.5$ and $\rho = 0.2$ for favorable and unfavorable combination, respectively.

The profiles of NB heating and CD for type A and the three off-axis NBIs with favorable combination are shown in Fig. 8. The total values of NB heating and CD are listed in Table 1. The total deposition powers of type A and type B NBIs are almost the same and are larger than those of type C and D NBIs. The off-axis NBI does not degrade the total current drive. Among the off-axis NBIs, the total current and deposition power of type B are highest. For type B, the profiles are well off-axis localized while for the other two off-axis types they are broadened. Therefore, type B is recommended for realizing off-axis NB heating and CD in EAST.

Fig. 9 shows the profiles of NBCD of type A and type B with favorable combination for beamline 1 and beamline 2. Beamline 1 is more tangential than beamline 2, so more trapped particles are produced with beamline 2. The magnitudes of NBCD with beamline 1 are doubled and peak a little outwardly compared with those with beamline 2. Therefore, beamline 1 is recommended for realizing off-axis NBCD in EAST.

3.2. The capability to control MHD activities

Off-axis NBI has been used to investigate sawtooth behavior in JET [8], MAST and ASDEX-U [9]. By drift kinetic modeling, they have found that the stability of $n = 1$ internal kink mode, which is thought to be related to sawtooth instability, is destabilized by the passing ions born outside the $q = 1$ rational surface due to the NBI. They successfully enhanced the fast ion effect by optimizing the deposition of the off-axis beam energetic particle population with respect

Table 1
The total values of NB heating and CD for four types.

Types	A	B	C	D
The total values of NBCD (kA)	89.47	97.89	93.68	88.55
The NBI power deposition to ions (MW)	0.9669	0.9419	0.8662	0.8782
The NBI power deposition to electrons (MW)	0.5446	0.5363	0.5132	0.5237

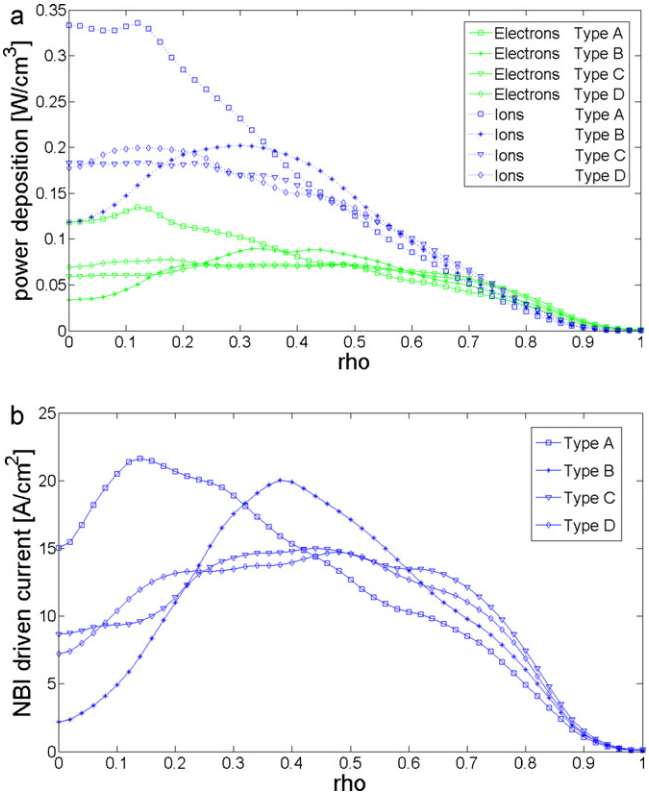

Fig. 8. The profiles of NBI power deposited (a) to electrons (green, solid) and ions (blue, dashed) and the profiles of NBCD, (b) for type A, B, C and D with co-NBI and the favorable combination of the toroidal magnetic field B_t and NB injection direction for NBCD. (For interpretation of the references to color in this figure legend, the reader is referred to the web version of the article.)

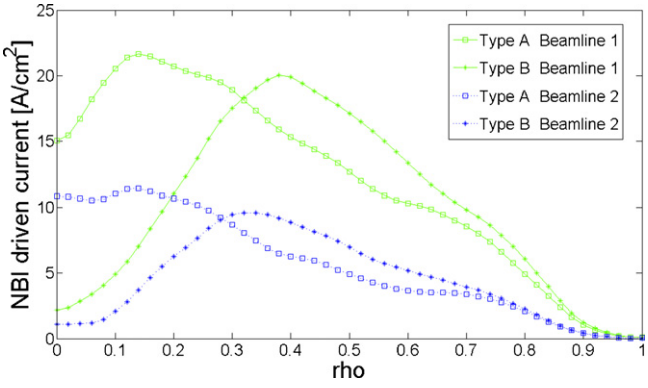

Fig. 9. The profiles of NBCD of type A and B for beamline 1 (green, solid) and beamline 2 (blue, dashed) with co-NBI and the favorable combination the toroidal magnetic field B_t and NB injection direction for NBCD. (For interpretation of the references to color in this figure legend, the reader is referred to the web version of the article.)

to the mode location. When the beam ions are deposited outside the $q = 1$ rational surface, the sawtooth period decreases. Profiles shown in Fig. 10 of safety factor and fast ion density for EAST with on- (Type A) and off- (Type B) axis NB are calculated by ONETWO.

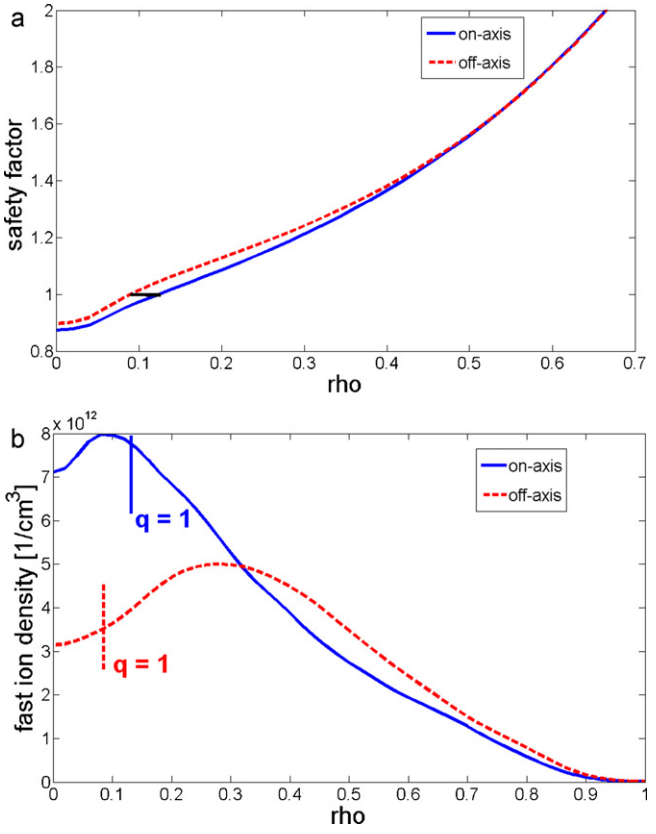

Fig. 10. The profiles of safety factor (a) and fast ion density (b) with on- (blue, solid) and off- (red, dashed) axis NBI. The inward shift of the q = 1 rational surface are shown in (a). In (b), the vertical solid and dashed lines indicate the locations of the $q = 1$ rational surface for on- (blue, solid) and off- (red, dashed) axis NBI, respectively. (For interpretation of the references to color in this figure legend, the reader is referred to the web version of the article.)

Both sources with the total beam power of 4 MW are considered here, and the temperature and density profiles introduced in Section 2.2 are used. For on-axis NBI, the $q = 1$ rational surface is located at $\rho = 0.13$ while the profile of fast ion density peak at $\rho = 0.09$, inside the $q = 1$ rational surface. When off-axis NBI is considered, the safety factor profile is changed and the $q = 1$ rational surface moves inward to $\rho = 0.09$. The profile of fast ion density peak at $\rho = 0.3$, outside the $q = 1$ rational surface. The fast ion density inside the $q = 1$ rational surface decreases significantly while the fast ion density outside the $q = 1$ rational surface increases. Therefore, according to the investigations in ASDEX-U, MAST and JET, by utilizing off-axis NBI we should be able to control sawtooth behavior in EAST.

4. Conclusion

Three different approaches to achieve off-axis NBI for EAST have been investigated and compared with on-axis NBI numerically by NUBEAM, a subroutine of ONETWO transport code. We find that the profiles of off-axis NBCD are sensitive to the alignment and there are some combinations of the toroidal magnetic field B_t and NB injection direction that are more favorable than others. For co-NBI, $+B_t$/down and $-B_t$/up are the most favorable combinations for

NBCD and $-B_t$/down and $+B_t$/up are the most favorable combinations for NB heating. For counter-NBI, the favorable combinations for NB heating and CD are the same, $+B_t$/down and $-B_t$/up. The off-axis NBI does not degrade the total current drive. Among the three approaches to realize off-axis NB heating and CD, the total current and deposition power are highest using type B and the profiles are well localized off-axis in contrast to the other two approaches in which the profiles are broadened. The numerical results for beamline 1 and beamline 2 have been compared. The magnitudes of NBCD with beamline 1 are doubled and peaked a little outwardly compared with those excepted with beamline 2. Therefore, type B and beamline 1 are recommended for off-axis NB heating and CD in EAST.

The capability to control sawtooth in EAST with off-axis NBI is confirmed by comparing locations of the $q = 1$ rational surface and the peak of fast ion density profile. More works have to be done, both numerically and experimentally, to insure a thorough understanding of the experimental results obtained after the NBI system is installed in EAST. This will be especially the case when Phase 2 (cf. Fig. 1) is installed. Then, the total NBI power can reach 8 MW and the effect of introducing an anomalous fast ion diffusion coefficient will have to be considered and investigated by comparing numerical results and experiment results.

Acknowledgments

One of the authors, Zhongjing Chen, would like to thank Qionglin Ni for the help in running the code. This work is supported by the State Key Development program for Basic Research of China (Nos. 2008CB717803, 2009GB107001, and 2007CB209903) and the National Natural Science Foundation of China (No. 10875002) in China.

References

[1] T. Suzuki, et al., Nucl. Fusion 51 (2011) 083020.
[2] J. Hobirk, et al., Proc. 30th EPS Conf. on Controlled Fusion and Plasma Physics, St. Petersburg, Russia vol. 27A (ECA) O-4.1B, 2003, http://epsppd.epfl.ch/StPetersburg/start.html.
[3] Sibylle Gunter, et al., 31st EPS Conference on Plasma Phys. Tarragona, 28 June – 2 July 2004 ECA Vol.28G, O-1.02 (2004).
[4] Sibylle Gunter, et al., 32nd EPS Conference on Plasma Phys. Tarragona, 27 June – 1 July 2005 ECA Vol.29C, P-4.075 (2005).
[5] J.M. Park, et al., Phys. Plasma 16 (2009) 092508.
[6] M. Murakami, et al., Nucl. Fusion 49 (2009) 065031.
[7] T. Suzuki, et al., Nucl. Fusion 48 (2008) 045002.
[8] I.T. Chapman, et al., Plasma Phys. Controlled Fusion 50 (2008) 045006.
[9] I.T. Chapman, et al., Phys. Plasma 16 (2009) 072506.
[10] J. Li, B. Wang, for the EAST Team and International Collaborators, Nucl. Fusion 51 (2011) 094007.
[11] Q. Ni, et al., Plasma Sci. Technol. 12 (2010) 661.
[12] B. Wu, et al., Fusion Eng. Des. 86 (2011) 947.
[13] S. Wu, EAST Team, Fusion Eng. Des. 82 (2007) 463.
[14] Hu C. and the EAST Team, Development of Long Pulse Neutral Beam Injector System for the EAST tokamak. Presented at the Ann. Conf. Of Chinese Nuclear Society, Beijing, China, Chinese Nuclear Society, Beijing. G01-0009, 2009.
[15] L. Terzolo, et al., J. Korean Phys. Soc. 58 (2011) 1091–1096.
[16] A. Pankin, G. Bateman, R. Bundy, et al., Comput. Phys. Commun. (2004) 164.
[17] NUBEAM Help, http://w3.pppl.gov/~pshare/help/nubeam.htm.
[18] H.E. St John, T.S. Taylor, Y.R. Lin-Liu, A.D. Turnbull, Proc. 15th Int. Conf. on Plasma Physics and Controlled Nuclear Fusion Research, (Seville, 1994) vol. 3 Vienna: IAEA, 1994, p. 603.
[19] W.W. Heidbrink, et al., Plasma Phys. Controlled Fusion 51 (2009) 125001.
[20] P. Helander, R.J. Akers, L.G. Eriksson, Phys. Plasma 12 (2005) 112503.